University Library

A gateway to Melbourne's research publications

Minerva Access is the Institutional Repository of The University of Melbourne

Author/s:
Choong, JK;Hampson, AJ;Brody, KM;Lo, J;Bester, CW;Gummer, AW;Reynolds, NP;O'Leary, SJ

Title:
Nanomechanical mapping reveals localized stiffening of the basilar membrane after cochlear implantation: Basilar membrane stiffness after CI

Date:
2020-01-01

Citation:
Choong, J. K., Hampson, A. J., Brody, K. M., Lo, J., Bester, C. W., Gummer, A. W., Reynolds, N. P. & O'Leary, S. J. (2020). Nanomechanical mapping reveals localized stiffening of the basilar membrane after cochlear implantation: Basilar membrane stiffness after CI. Hearing Research, 385, https://doi.org/10.1016/j.heares.2019.107846.

Persistent Link:
https://hdl.handle.net/11343/247873

License:
CC BY-NC-ND

Hearing Research 385 (2020) 107846

Contents lists available at ScienceDirect

Hearing Research

journal homepage: www.elsevier.com/locate/heares

Nanomechanical mapping reveals localized stiffening of the basilar membrane after cochlear implantation

Jessica K. Choong [a], Amy J. Hampson [a], Kate M. Brody [a], Jonathon Lo [a], Christofer W. Bester [a], Anthony W. Gummer [b], Nicholas P. Reynolds [c, d, **], Stephen J. O'Leary [a, *]

[a] Otolaryngology, Department of Surgery, University of Melbourne, Royal Victorian Eye and Ear Hospital, East Melbourne, Australia
[b] Section of Physiological Acoustics and Communication, Department of Otolaryngology, Eberhard-Karls-University Tübingen, Elfriede-Aulhorn-Strasse 5, 72076, Tübingen, Germany
[c] ARC Training Centre for Biodevices, Swinburne University of Technology, Hawthorn, Australia
[d] Department of Chemistry and Physics, La Trobe Institute for Molecular Science, La Trobe University, Australia

ARTICLE INFO

Article history:
Received 19 June 2019
Received in revised form
2 November 2019
Accepted 10 November 2019
Available online 16 November 2019

Keywords:
Cochlear implantation
Hearing loss
Atomic force microscopy
Basilar membrane
Fibrosis

ABSTRACT

Cochlear implantation leads to many structural changes within the cochlea which can impair residual hearing. In patients with preserved low-frequency hearing, a delayed hearing loss can occur weeks-to-years post-implantation. We explore whether stiffening of the basilar membrane (BM) may be a contributory factor in an animal model. Our objective is to map changes in morphology and Young's modulus of basal and apical areas of the BM after cochlear implantation, using quantitative nanomechanical atomic force microscopy (QNM-AFM) after cochlear implant surgery. Cochlear implantation was undertaken in the guinea pig, and the BM was harvested at four time-points: 1 day, 14 days, 28 days and 84 days post-implantation for QNM-AFM analysis. Auditory brainstem response thresholds were determined prior to implantation and termination. BM tissue showed altered morphology and a progressive increase in Young's modulus, mainly in the apex, over time after implantation. BM tissue from the cochlear base demonstrated areas of extreme stiffness which are likely due to micro-calcification on the BM. In conclusion, stiffening of the BM after cochlear implantation occurs over time, even at sites far apical to a cochlear implant.

© 2019 The Authors. Published by Elsevier B.V. This is an open access article under the CC BY-NC-ND license (http://creativecommons.org/licenses/by-nc-nd/4.0/).

1. Introduction

Cochlear implantation results in a spectrum of microscopic changes within the cochlear anatomy including fibrosis and osteoneogenesis, particularly concentrated within the basal end of the cochlea adjacent to the implant array. This is seen both in humans (Li et al., 2007; Linthicum et al., 2017; Nadol et al., 2001; Fayad et al., 2009) and in experimental models of implantation (O'Leary et al., 2013). These changes are thought to affect cochlear mechanics (Choi and Oghalai, 2005; Kiefer et al., 2006) and subsequently the recipient's hearing. Patients with residual low-frequency hearing are deemed eligible for cochlear implantation with electro-acoustic stimulation (EAS) models of implants. In an attempt to preserve this hearing, current surgery has focused upon "soft-surgical" techniques (Lehnhardt, 1993), implant design (Gantz et al., 2005; Briggs et al., 2013) and intraoperative monitoring (Campbell et al., 2016).

Delayed hearing loss in EAS recipients refers to the hearing loss which can develop some months after implant insertion, as reported by recipients and confirmed on audiometric testing. This typically occurs weeks-to-months, and in some cases years, post-implantation (Gstoettner et al., 2006). Choi and Oghalai (2005) proposed that one mechanism by which delayed hearing loss might occur was damping of scala tympani by fibrosis, or immobilization of the basilar membrane (BM) by fibrosis and/or direct contact with the CI. Here, we explore an alternative hypothesis, namely that delayed hearing loss results from variations in cochlear

* Corresponding author. Otolaryngology, Department of Surgery, Royal Victorian Eye and Ear Hospital, 32 Gisborne Street, East Melbourne, 3002, Australia.
** Corresponding author. Department of Chemistry and Physics, La Trobe Institute for Molecular Science, La Trobe University, Science Drive, Bundoora, Vic, 3083, Australia.
E-mail addresses: nicholas.reynolds@latrobe.edu.au (N.P. Reynolds), sjoleary@unimelb.edu.au (S.J. O'Leary).

https://doi.org/10.1016/j.heares.2019.107846
0378-5955/© 2019 The Authors. Published by Elsevier B.V. This is an open access article under the CC BY-NC-ND license (http://creativecommons.org/licenses/by-nc-nd/4.0/).

mechanics caused by progressive changes to the Young's modulus of the BM over time. The latter could arise as a late consequence of cochlear inflammation and subsequent micro-calcification. BM stiffness and/or Young's modulus has been measured previously in the guinea pig (Gummer et al., 1981; Miller, 1985) and other species including humans (Von Békésy, 1960; Olson and Mountain, 1991; Olson and Mountain, 1994; Naidu and Mountain, 1998; Emadi et al., 2004; Emadi and Richter, 2008; Teudt and Richter, 2014). However, none so far have looked specifically at the impact of cochlear implantation on BM stiffening.

Here, we looked specifically for changes in the Young's modulus of guinea pig BM tissue at multiple time points following cochlear implantation surgery using Quantitative NanoMechanical Atomic Force Microscopy (QNM-AFM). QNM-AFM allows simultaneous mapping of the Young's moduli and topography of biological materials in fully hydrated conditions with nanometer resolution (Gilbert et al., 2017), accounting for the significant heterogeneity seen in biological tissue. Traditional methods of quantifying mechanical properties of materials by AFM [e.g., by analyzing individual force vs distance curves (Kuznetsova et al., 2007)] lack the ability to map with nanometer spatial resolution and, thus, are unable to correlate changes in material properties with sub-micron variations in topography. This limitation has prevented correlative studies which investigate relationships between changing mechanical and morphological properties in biological tissues. Here, for the first time, we perform nanoscale correlative mapping of the BM, allowing us to monitor progressive nanoscale changes in BM topography and Young's modulus as a result of cochlear implantation. These changes in biophysical properties were further investigated audiometrically.

We show that the apical BM region – far away from the implant – becomes progressively stiffer with time after implantation. QNM-AFM suggest this stiffening is likely due to collagen deposition on the tympanic surface of the BM.

2. Materials and methods

2.1. Animals and experimental design

All experimental procedures were in accordance with the Bionics Institute's Animal Research Ethics Committee (ethics approvals 16/354AU and 16/360AU). Fifty pigmented Dunkin-Hartley guinea pigs were used in this study, from which data are presented for 38 animals (weight range 437–974 g); the remainder were used for either preliminary experiments or were accidently damaged during AFM sample preparation (see Table 1). Animals were aged 8–20 weeks at the time of cochlear implantation. Experimental animals were divided into four groups of ten, with designated survival endpoints of 1, 14, 28, and 84 days. All animals allocated to these experimental groups underwent baseline auditory brainstem response (ABR) testing prior to bilateral cochlear implantation via cochleostomy, followed by repeat ABR recordings at their designated survival end-point. Five animals were designated as controls, and these had no surgical intervention. All cochleae were removed and underwent BM dissection for AFM. All surgery was performed by one surgeon (JC) and the researchers were blinded for AFM analysis.

2.2. Auditory brainstem response recordings

Anaesthesia for ABR recordings and surgery was inducted with intramuscular ketamine (60 mg/kg) and xylazine (4 mg/kg). Animals were maintained in an areflexic state throughout all procedures, as determined by lack of both pedal and corneal reflexes. Our ABR recording system has been previously described (James et al., 2008). Computer-generated acoustic stimuli (100 μs clicks and tone pips of duration 5 ms, with 1 ms rise/fall times and stimulus frequencies of 2, 8, 16, 24 and 32 kHz) were delivered to each ear via a loudspeaker (Richard Allen DT-20, UK) placed 10 cm away from the pinna. Ear mould compound (Otoform, Dreve, Germany) was used to occlude the contralateral ear. Subcutaneous needle electrodes were placed at the vertex and ipsilateral nape of the animal with a ground electrode placed subcutaneously in the flank. Responses were amplified by a factor of 100,000 (DAM-5A, WPI Inc., USA) and band-pass filtered (Krohn-Hite 3750, Avon, USA) between 150 Hz and 3 kHz (6 dB/octave). The filter output was fed to a 16-bit analogue-to-digital converter (Tucker Davis Technologies, USA) and sampled at 20 kHz for a period of 10 ms following stimulus onset. Thirty stimuli were presented per second. Responses were averaged over 250 stimulus repetitions. Stimulus intensity was decremented in 5 dB steps from high to sub-threshold stimulus levels. Waveforms were exported to a software analysis program (written by Dr. James Fallon and adapted by Prof. Stephen O'Leary using Igor 5.02, Wavemetrics Inc., USA), with threshold defined as the lowest intensity stimulus to evoke a response of >0.4 μV amplitude in wave III of the ABR. ABRs were recorded on the day of cochlear implantation (prior to the commencement of the surgical procedure), and were repeated at the endpoint of each experiment (1, 14, 28 or 84 days, dependent on experimental group).

2.3. Surgery

Lignocaine (1 mg/mL) was injected subcutaneously prior to post-auricular incision. Overlying tissue was mobilized off the bulla and a 1.8 mm cutting burr was used to form a bullostomy. A cochleostomy was created using a 0.8 mm diamond burr approximately 1 mm from the round-window membrane in an antero-inferior plane (Lo et al., 2017). A non-stimulating dummy silicone implant, manufactured in our laboratories using SILASTIC® MDX4-4210 BioMedical Grade Elastomer (Dow Corning Products, USA), with a diameter of 0.4 mm was then slowly and carefully inserted into the cochlea to a depth of ~2.5 mm, unless resistance was felt earlier. The dummy implant was left in place and trimmed at the level of the bullostomy. The cochleostomy was sealed with a muscle plug and the muscle overlying the bulla was re-approximated and sutured. The post-auricular skin was sutured and the incision site

Table 1
Animal numbers analysed by AFM in each cohort with group mean stiffness. NB: Some specimens were destroyed during sample preparation and AFM analysis resulting in groups consisting of varying numbers.

Cohort	Apical AFM		Basal AFM	
	Number of animals	Group median stiffness (kPa)	Number of animals	Group median stiffness (kPa)
Control	5	55	5	65
1 day	9	61	8	94
14 days	7	127	9	101
28 days	9	219	8	145
84 days	8	259	7	146

sprayed with tissue adhesive. All animals were then given a subcutaneous injection of an analgesic (Temgesic, Reckitt Benckiser, Australia) and allowed to recover from anaesthesia.

Silicone non-stimulating arrays were chosen over Pt/Ir electrode arrays for two reasons. First, the aim was to investigate changes in BM stiffness over time due to the presence of the implant. Further studies investigating the effect of electrical stimulation whilst no doubt of significant interest were beyond the scope of this study. Second, silicone implants have been used in comparable studies in our laboratory (Choong et al., 2019) and their continued use allows for more reliable comparison of results between studies.

2.4. Cochleae harvesting and preparation

Whilst still under anaesthesia and following the final ABR recording, animals were euthanized with an intraperitoneal injection of pentobarbitone (2.5 mL; 325 mg/mL). Transcardiac perfusion with heparinized normal saline followed by 10% neutral buffered formalin was performed to allow cochleae to be harvested. After harvesting, right-side cochleae were placed into phosphate-buffered saline (PBS) solution and stored at 4 °C until BM dissection.

BM dissection occurred under a microscope within 2 h of harvesting the cochleae. Cortical bone and the otic capsule were carefully chipped away in order to expose the BM. Two BM samples approximately 2 mm in length were collected – a basal sample from the region adjacent to the cochleostomy, and an apical sample adjacent to the helicotrema. The spiral ligament was removed in all samples, though a small remnant border of the modiolus was retained on both samples for structural integrity. Dissected BM were then placed on glass coverslips pre-treated with Fol's Chrome Alum Gelatin coating to prevent lifting of the samples during AFM measurement. Slides were stored at 4 °C for a maximum of three days prior to AFM analysis.

2.5. Quantitative Nanoscale Mechanical-Atomic Force Microscopy (QNM-AFM)

Tissue samples were characterised by QNM-AFM on a MultiMode 8 AFM with a NanoScope V Controller (Bruker). All imaging was performed using the fluid cell in PBS at room temperature. ScanAsyst-Fluid (Bruker) cantilevers were used with a nominal spring constant of 0.7 N/m and resonant frequency of 150 kHz in air. A schematic of the operation of QNM-AFM is shown in Fig. 1. In QNM-AFM, similarly to tapping mode, an oscillating AFM tip is rastered across the substrate, and a topographic image is generated by monitoring the lateral displacement of the cantilever for every pixel of the generated image. In addition, for each pixel the force exerted on the tip by the substrate is measured throughout the oscillation of the tip (Fig. 1, bottom), generating a force vs distance curve for each pixel (Fig. 1, top). The Young's modulus at each pixel was then calculated by numerically fitting this force vs distance curve in its deformative (*Def.*) region using the Derjaguin-Muller-Toporov (DMT) mechanical model for elastic contact (Fig. 1, red line, top right) (Young et al., 2011), thereby generating a nanoscale map of the Young's modulus variation of the BM. To produce these nanomechanical maps, all imaging was performed in peak-force tapping mode where the cantilever was oscillated at a frequency of 0.5 kHz, chosen to be much lower than its resonant frequency.

Before imaging, each cantilever was calibrated to accurately determine the deflection sensitivity, spring constant, and the tip radius. Deflection sensitivity was calculated from a force-distance curve generated by indenting the tip into a hard, fused silica surface. The spring constant was determined in both air and PBS using the thermal tune procedure included in the NanoScope Control software (V1.4, Bruker). Briefly, a thermal noise spectrum is generated by monitoring small thermal oscillations of the cantilever over a range of frequencies. This thermal noise spectrum can then be used to numerically calculate the resonant frequency and the spring constant of the cantilever (Lübbe et al., 2013). The tip radius was calculated by analysis of a 1.5 μm scan of the roughened titanium control sample (Bruker, RS-12M) using the tip analysis tool in the NanoScope Analysis software (V1.7, Bruker). To further refine the calibration, 3 × 3 μm^2 scans of a polydimethylsiloxane film of known Young's modulus (nominally 2.5 MPa; Bruker PDMS-SOFT-1-12M) were imaged and the calculated tip radius adjusted so the measured Young's modulus matched the nominal stiffness of

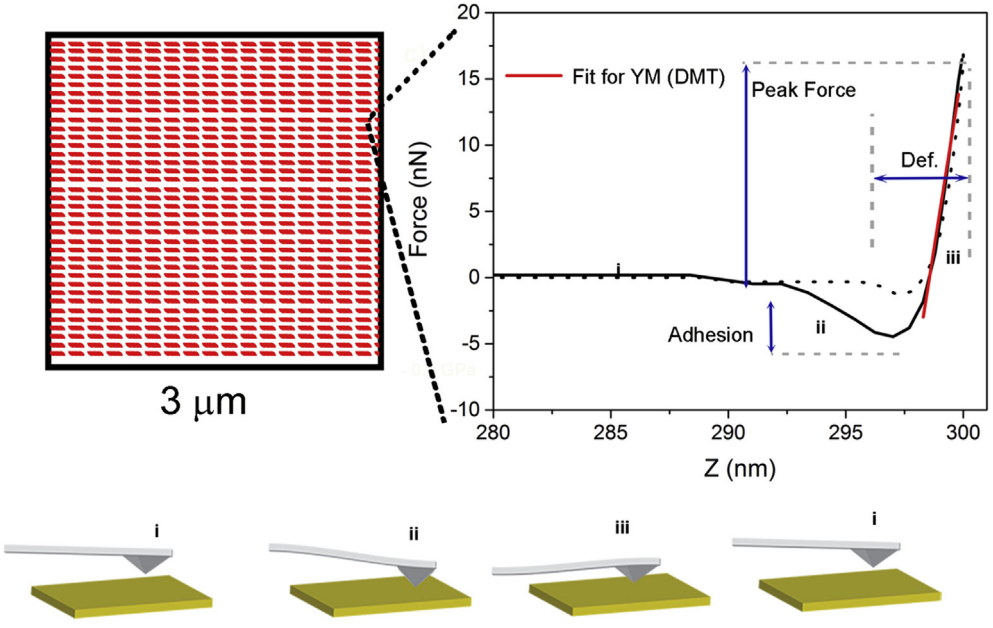

Fig. 1. Schematic of the operation of Quantitative Nanoscale Mechanical-Atomic Force Microscopy.

the calibration sample. Using this estimation procedure, the effective tip radius was calculated to be typically around 30 nm. When scanning, the deformation channel was monitored carefully to ensure that the maximum indentation into the BM did not exceed 10 nm, thus minimizing any substrate influence on the calculated Young's modulus (Chung et al., 2014). Nanoscale deviations from planarity in the prepared substrates were subtracted from the topographical maps using the 1st order Flatten tool in the NanoScope Analysis software; no further processing was performed. (Note: DMT modulus quantification was chosen as it routinely provided less noisy, more repeatable data than Sneddon modulus quantification, ostensibly because the maximum indentation depth was chosen to be no more than about the tip radius.)

Between three and six points within the pars pectinata of the BM were measured in each tissue sample; fewer measurements were achievable when tissue was lifted from the glass plate by the AFM tip and, therefore, was no longer suitable for repeated measurements. All recordings were taken from areas as close as possible to the medial border of the BM to ensure testing repeatability. Median Young's modulus of each specimen was used for comparison between cochleae.

2.6. Statistical analyses

AFM force maps were exported as American Standard Code for Information Interchange (ASCII) files using the open source AFM analysis software Gwyddion (v.2.41) and then subsequently imported into Microsoft Excel. The median stiffness for each animal was found and these measurements were imported into IBM SPSS Statistics (v.25) for statistical analysis. Kruskal-Wallis tests were performed for intergroup comparisons. ABR data were analysed in SPSS with mixed-model ANOVA. These data were graphed in Matlab (v.16b).

3. Results

3.1. Hearing thresholds before and after implantation

The pre-implant ABR thresholds are presented in Fig. 2a, revealing thresholds within anticipated levels for normal hearing guinea pigs. These data were analysed by a mixed model ANOVA. Although these thresholds differed across stimulus frequency ($F_{(4,136)} = 59.0$, $p < 0.01$), they did not by study group (each of which survived a different period of time after implantation, $F_{(3,\ 34)} = 1.28$, $p = 0.30$). There was an association between frequency and study group, as evidenced by an interaction between these factors in the linear model ($F_{(12,132)} = 2.18$, $p = 0.02$), but simple effects testing (with ANOVA) by frequency did not reveal an explanation for this association.

ABR threshold shifts revealed that hearing deteriorated across stimulus frequency immediately after implantation (Fig. 2b). When subjected to a mixed-model ANOVA, threshold shifts were found to differ across frequency ($F_{(4,136)} = 22.0$, $p < 0.01$), and there was an interaction between frequency and the study group (i.e. days' survival; $F_{(12,132)} = 2.81$, $p = 0.002$). Post-hoc testing showed that this association could be accounted for by a significantly greater 8 kHz threshold shift at 28 days than at day 1 (Tukey's honestly significant difference test, $p = 0.009$), with other frequencies following this trend. Threshold at 2 kHz (the most distant frequency from the site of implantation) was the least affected by cochlear implantation, with threshold shifts one day after surgery demonstrating a mean threshold loss of 7 dB, which rose progressively to peak by 84 days at 14 dB. These threshold shifts did not differ significantly over survival time ($F_{(3,34)} = 0.8$, $p = 0.50$).

3.2. Basilar-membrane stiffness using QNM-AFM

3.2.1. Topography and stiffening of basilar membrane from the basal cochlea

The BM at the base of the cochlea became progressively stiffer after implantation, rising from a cohort median Young's modulus of 94 kPa (IQR = 53) one day after implantation to 146 kPa (IQR = 123) at 84 days (Fig. 3). Control animals had a median Young's modulus of 65 kPa. The difference in Young's moduli across time was not statistically significant (Kruskal Wallis, *Chi square* = 5.734, $p = 0.220$, df = 4).

The stiffness outcomes were accompanied by a subtle change in the observed topography of the basal BM (Fig. 4). At 28 days (Figs. 4e) and 84 days (Fig. 4g), punctate, particulate features on the BM were observed (example features highlighted by red arrows in Fig. 4e and g), which are not present at earlier time points. These punctate spots were approximately 100 nm in diameter and possessed higher Young's modulus (approximately 2 MPa) (Fig. 4f and h) than the median BM in this cohort (146 kPa) (Fig. 4b and d). Representative topographical and stiffness maps of BMs from control animals are shown in the Supplementary material. In general, the topographical AFM images of the non-implanted animals look very similar to the AFM images recorded both 1 and 14 days post-implantation. Contrary to the 84 day cohort, corrugation of nano-particulate features was not found.

More dramatic mechanical and topographical changes were seen in three of the studied animals in the 84 day cohort. These animals were found to possess areas of exceptionally high Young's modulus (exceeding the 10 MPa detection limit of the probe). The

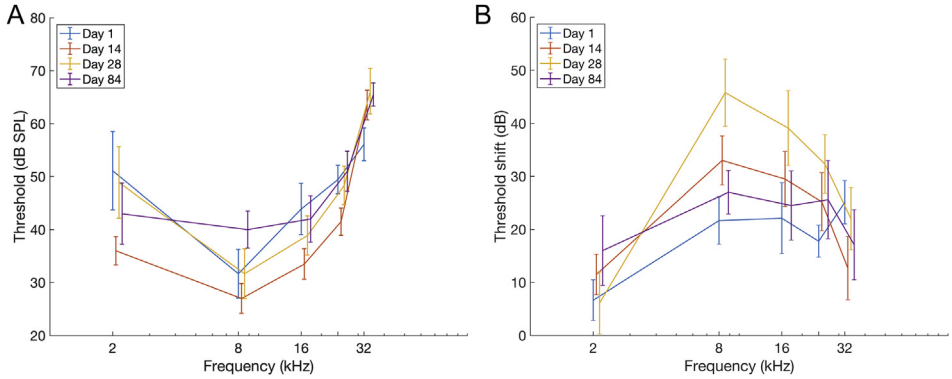

Fig. 2. a) Pre-operative ABR thresholds [mean with standard error of the mean grouped by study cohort (days' survival)], **b)** ABR threshold shifts at the end of the survival period for each group (mean and standard error of the mean).

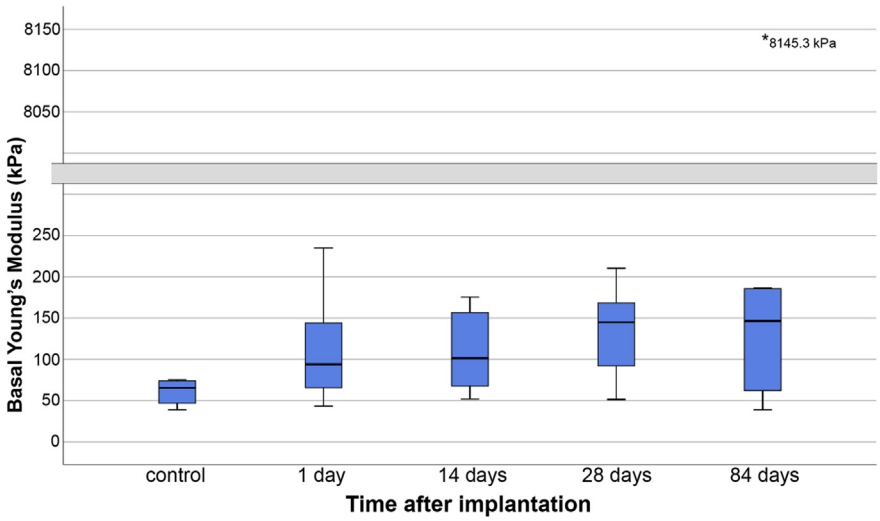

Fig. 3. Young's modulus of the basal BM over time as measured by QNM-AFM (median, inter-quartile range [box] and range). There was one outlier in the 84 day cohort with an exceptionally high Young's modulus (8145 kPa) compared with all other animals in this study.

stiff areas were seen in the modulus channel as areas of saturated intensity intermingled with tissue resembling its original appearance (Fig. 5). This area occupied 8.79% of the recorded surface of the 84 day group (compared with all other groups presenting less than 0.02% surface area) and were assigned a value of 10 MPa for the statistical analysis performed in Fig. 3.

The topography of these very stiff regions looked markedly different to the topography of the rest of the tissue analysed. Two dominant topographical features were observed. The first common feature, despite its much increased stiffness (Fig. 5e and f), had a topography (Fig. 5d) similar to the nanoparticulate features seen in Fig. 4g. Fig. 5d–f showed an evenly distributed layer of very stiff nanoparticles with diameters around 100 nm (Fig. 5d–f, red arrows). These nanoparticles resemble, in both size and shape, features previously attributed to hydroxyapatite crystals seen by AFM in trabecular bone samples (Hassenkam et al., 2004; Thurner et al., 2007). The second feature had a fibrillar topography with perpendicular striations (Fig. 5a–c & 5g–I, green arrows) displaying a 67 nm banding (Fig. 6) characteristic of collagen fibers (Hassenkam et al., 2004).

3.2.2. Topography and stiffening of basilar membrane from the apical cochlea

The apex of the cochlea showed progressive stiffening of the BM after implantation, with the 84 day cohort peaking at 259 kPa (IQR = 201), having risen from 60 kPa (IQR = 36) one day after implantation (Fig. 7). Non-implanted control animals had a median Young's modulus of 55 kPa. The difference across groups including the controls was statistically significant (Kruskal Wallis: *Chi square* = 18.001, df = 4, $p = 0.001$). Post-hoc analysis (Dunn's test with Bonferroni correction) showed a significant difference between the control and 28 day cohorts ($p = 0.003$), 1 day and 84 day cohorts ($p = 0.003$), and the 1 day and 28 day cohorts ($p = 0.001$).

Topographic imaging by QNM-AFM, revealed no apical regions that exceeded the maximum modulus measurable by the AFM tips used (10 MPa); however, there was a progressive change in the structural organization of the tissue resulting in the development of bundles of fibrillar structures over time (Fig. 8).

Quantification based on analysis of line sections drawn through the bundles of fibrils at 84 days (Fig. 9) revealed them to be distinctly stiffer than the median modulus of the BM at the same time point. The mean Young's modulus of these fibrils at 84 days was 629 ± 15 kPa, more than twice the median from this cohort (259 kPa).

4. Discussion

By using the QNM-AFM technique we were able to simultaneously map – with nanoscale precision – changes in tissue topography and mechanical properties resulting from the presence of a simulated CI in scala tympani. This mapping allowed correlation of nanoscale changes in topography with corresponding changes in Young's modulus.

4.1. Young's modulus for the basilar membrane of non-implanted cochleae

Non-implanted control animals were found to possess a Young's modulus varying between 32 and 78 kPa (median 55 kPa) in apical regions of the BM and 38–75 kPa (median 64 kPa) in the basal regions. In the absence of similar experiments for the guinea pig BM, we make comparisons with experimentally determined values of Young's modulus from the *in-situ* BM and tectorial membrane (TM) of mice and also the isolated TM of guinea pigs. Using a contact probe and quasi-static measurement of point stiffness in a hemi-cochlear preparation from the CBA/CaJ mouse, the Young's modulus of the BM was calculated to vary between 13 and 200 kPa in basal regions and 3–25 kPa in apical regions, and for the TM between 5 and 100 kPa in basal regions and 0.4–4 kPa in apical regions (Teudt and Richter, 2014). Using a non-contact probe and acoustic stimulation of isolated TM from the guinea pig cochlea, the mean Young's modulus of the TM was reported to vary from 14 kPa in basal regions to 3 kPa in apical regions (Gavara and Chadwick, 2010). In other words, all of the experiments suggest that Young's modulus is larger for the BM than the TM. Given that Naidu and Mountain (1998) have demonstrated experimentally that the structures overlying the BM contribute about one half of the *in-situ* BM stiffness measured in the pectinate zone under the outer hair cells (in the basal turn), Young's modulus values for *isolated* BM from CBA/CaJ mouse would be predicted to be about one half of those derived from the mouse hemi-cochlear preparation. Therefore, our modulus values for guinea pig BM isolated from the basal region, being about half those from the basal BM region of the mouse hemi-cochlear preparation, engender confidence that the

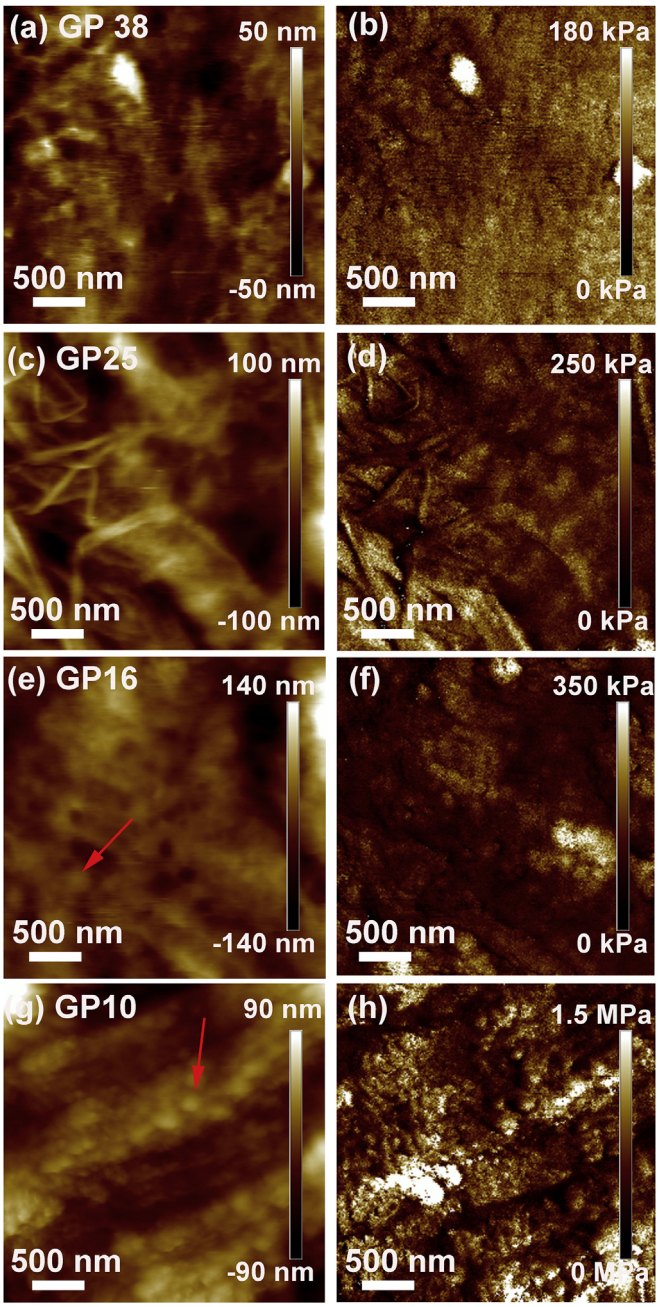

Fig. 4. QNM-AFM topography (a,c,e,g) and Young's modulus maps (b,d,f,h) of the basal basilar membrane of animals from 1 day (a,b), 14 days (c,d), 28 days (e,f), and 84 days (g,h) cohorts. Red arrows represent stiffer nano-particule features that appear on the BM after 28 days. *GP* is an animal identifier.

dissection and sample preparation did not significantly alter the Young's modulus of the BM tissue sections. However, in contrast to the order of magnitude decrease of Young's modulus from base to apex for the BM and TM reported in the hemi-cochlear preparation (Teudt and Richter, 2014), we did not detect a significant decrease for the isolated BM. The most parsimonious explanation for the difference is that the modulus estimates in the hemi-cochlear preparation are strongly influenced by the geometry and boundary conditions of the *in-situ* system. Furthermore, based on earlier experiments and models for the guinea pig BM (Gummer et al., 1981; Miller, 1985; Fleischer et al., 2010), modulus values in the tens of kPa range for both the hemi-cochlear preparation (Teudt and Richter, 2014) and our isolated BM preparation suggest that the major proportion of the measured modulus value – for the un-implanted cochlea – is due to the ground substance and tympanic cells of the BM. Specifically, from point forces applied with a contact probe, Miller (1985) estimated using a BM beam model that these two constituents have a Young's modulus of about 10 kPa, and Fleischer et al. (2010) estimated using a three-dimensional finite-element model that the ground substance has a Young's modulus of 100–200 kPa. The latter estimate is similar to what we measured in the present experiments for the un-implanted cochlea. In summary, our measured values of Young's modulus are consistent with expectations based on earlier theoretical and experimental reports, implying that the isolated BM preparation is biologically relevant.

4.2. Progressive stiffening of the basilar membrane with time after implantation

As time elapsed post-implantation, the Young's modulus of the BM increased, and the tissue morphology was altered, at both the base and apex of the cochlea. In the base of the cochlea, by 84 days there were numerous microscopic areas of very stiff (high Young's modulus) tissue. Two distinct features were seen in these very stiff regions. The first possessed a fibrous morphology with a regular 67 nm banding structure, and almost certainly indicates the deposition of bundles of collagen fibrils on the base of the BM (Hassenkam et al., 2004). The second features have a spherical nanoparticle-like morphology that look very similar to nanoparticles previously identified by AFM as hydroxyapatite crystals (Hassenkam et al., 2004; Thurner et al., 2007). The presence of hydroxyapatite crystals on the BM is likely due to excessive micro-calcification occurring at the base of the cochlea. Similar hydroxyapatite micro-calcification has been seen in a number of different tissues and pathologies including: nonvisceral and vascular soft tissues (Carlstrom et al., 1953), breast cancers (Sharma et al., 2016), renal calcification (Contiguglia et al., 1973), and the calcification of tendons (Anderson, 2003).

In contrast, in apical cochlear regions exceptionally stiff tissue similar to the bone-like tissue seen in the basal regions was not observed. Instead, the BM underwent a progressive change in tissue structure over time, to form discrete bundles of fibrils that are clearly present in the 24 and 84 day cohorts. These bundles of nanofibrils possessed a Young's modulus more than twice the median of the BM from the same cohort. Due to the nanofibrillar topography and also their increased Young's modulus, we believe these fibrils are also deposited bundles of collagen fibrils. However, the 67 nm corrugation was not observed in the bundles from the apex of the BM. The lack of corrugation in these fibrils can be attributed to a loss of lateral resolution in the AFM when imaging the softer tissue at the apex of the BM compared to the very stiff calcified regions in the base. Similarly, Thurner et al. (2007) reported that the 67 nm collagen fiber banding in bone was often impossible to resolve when imaging in a fluid environment. Further support for the hypothesis that the fibrillar structures seen for the 84 day cohort in the BM apex are collagen-based comes from previous published studies of extracellular tissue by AFM (Graham et al., 2010). They showed similar fibrillar structures in collagen-rich extracellular matrix tissue samples. Wenger et al. (2007) showed that the Young's modulus of individual collagen fibrils varied between 5 and 10 GPa, several orders of magnitudes higher than the median modulus of the BM. Hence, the presence of even small concentrations of collagen fibrils could potentially cause significant stiffening of the BM.

In the topographical images, the apical tissue at 1 day post-implantation appeared relatively homogenous and lacked distinctive structure compared with post-implantation animals at later

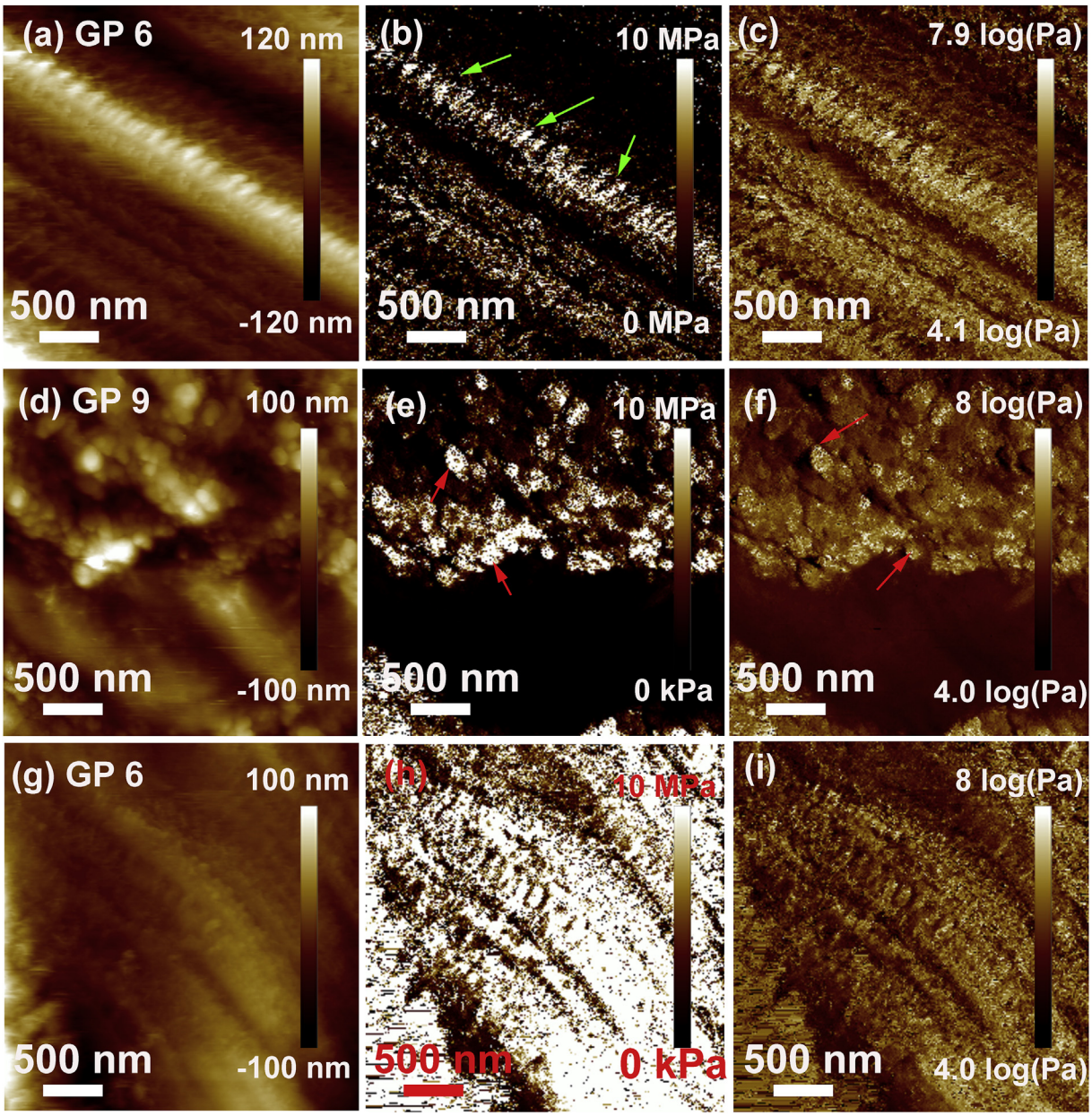

Fig. 5. Representative images of the extremely stiff tissue deposited on 8.79% of the area examined of the BM from the base of the cochlea showing topography (left), Young's modulus (centre) and log modulus (right). Note that the so-called log modulus, denoted by log*(Pa)* in the figure, is taken directly from the NanoScope software and means log(Young's modulus re. 1 Pa). The corrugated features (green arrows) in the top and bottom rows were likely due to collagen fibrils and the particulate features in the middle row (red arrows) were likely hydroxyapatite crystals; both have been associated with excessive micro-calcification in other systems. *GP* is an animal identifier.

time points, which may be due to early inflammatory changes including tissue edema and the influx of early inflammatory cells disrupting the usual homeostasis of the intracochlear fluid spaces. Tissue structures could be more clearly identified over time consistent with gradual resolution of the inflammatory process (Kel et al., 2013).

While this paper suggests that collagen deposition results along the *entire* cochlea after cochlear implantation, it is not yet understood why such deposition might occur. We propose two mechanisms that might be considered. The first is that either bleeding or impairment of the blood-labyrinthine barrier(s) leads to diffusion of pro-thrombotic factors from serum throughout the perilymphatic scalae, resulting in a widespread deposition of fibrin. This activation of the coagulation pathways would likely activate the fibroblasts, with the fibrin forming as a scaffold for the micro-scarring observed here. Alternatively, cochlear inflammation may have activated the fibroblasts directly, and promoted a pro-fibrotic response. Recent studies suggest that after injury, macrophages are activated for extended periods of time (Frye et al., 2018), and the same could potentially be true for fibroblasts.

In summary, the AFM results from the apical cochlea are consistent with a maturation of fibrosis over time. In many systems, this involves a progressive stiffening of the scar through contraction of myofibroblasts (Ehrlich and Hunt, 2012). So, we speculate that progressive stiffening of the micro-scar could explain the gradual stiffening of the BM.

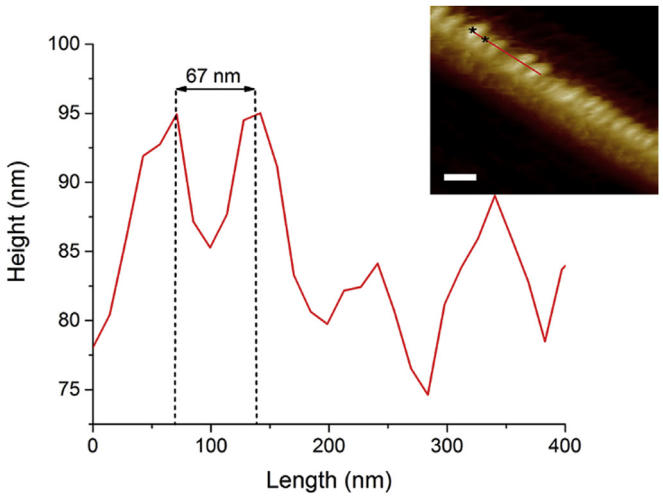

Fig. 6. AFM height profile of bundles of (presumably collagen) fibrils deposited on the basal region of the basilar membrane, displaying collagen-like banding with a 67 nm periodicity (z-scale of inset is 90 nm, scale bar = 200 nm). Images taken from the BM of GP 6.

4.3. Hearing loss in Guinea pigs

As has been seen in many other experimental models of cochlear implantation, ABR thresholds did not recover to pre-operative levels following cochlear implantation. The extent of permanent hearing loss varies between studies, and in both humans (Gantz et al., 2005) and animals (Stathopoulos et al., 2014), complete hearing preservation is possible. Our previous work has found an association between the extent of cochlear fibrosis and hearing loss (O'Leary et al., 2013). It is thought that the extent of cochlear inflammation and subsequent apoptosis (Eshraghi and Van De Water, 2006), the presence of blood within scala tympani (Radeloff et al., 2007; Ryu et al., 2015) and direct trauma to cochlear structures (O'Leary et al., 2013) are the main determinants of both fibrosis and hearing loss. While inflammation and fibrosis may be correlated with hearing loss, the reason(s) why these lead to permanent threshold elevation is not so clear. Inflammation predisposes to a loss of hair cells (Haake et al., 2009), and hair cell loss and threshold elevation are correlated in the vicinity of the cochlear electrode (O'Leary et al., 2013; Lee et al., 2013), but not in more apical cochlear regions responsible for lower-frequency hearing (Lee et al., 2013). To explain this "apical" hearing loss, other mechanisms must be proposed. The endocochlear potential is not sufficiently impaired after implant surgery to explain this loss (Oshima et al., 2014). Fibrosis provides a potential explanation: When the fibrosis is sufficient to dampen the scala tympani, hearing loss will be experienced throughout the cochlea (Choi and Oghalai, 2005), but this degree of fibrosis is seldom seen in animals. Fibrosis of the BM will cause hearing loss in the scarred region (Choi and Oghalai, 2005; Kiefer et al., 2006), but until now it has not been clear how fibrosis in the vicinity of a cochlear electrode might stiffen the BM more apically. We have shown that this does occur through micro-scarring, which means that BM stiffening could potentially contribute to hearing loss throughout the cochlea.

The results presented here provide a potential explanation for delayed hearing loss, which is frequently seen in humans after implant surgery. Delayed hearing loss occurs at low frequencies, meaning that the acoustic response is generated in cochlear regions apical to that of the implant electrode. The gradual deterioration in 2 kHz thresholds over time in this study is analogous. Fibrosis matures over time, and maturation of a fibrotic reaction takes several months, in keeping with the changes seen here by AFM. Increased stiffness might be expected to also increase the resonant frequency of the BM, and progressively reduce its sensitivity to low-frequency sounds, causing a delayed hearing loss. However, whether the AFM-derived modulus measurements cause these changes remains unclear. A significant correlation was not found between Young's modulus and ABR threshold shifts in this study; however, it should be noted that the apical section of BM used for QNM-AFM was from near the helicotrema and, therefore, was more apical than the 2 kHz cochlear place. Further studies performing QNM-AFM along the full length of the BM would be beneficial. It is apparent from this study that if fibrosis is related in any way to hearing loss that the time-period over which change may occur is months.

Peak hearing loss occurred at 28 days post-implantation in the 8–32 kHz range, but after 28 days these thresholds partially recovered. This has been observed in earlier studies (Lee et al.,

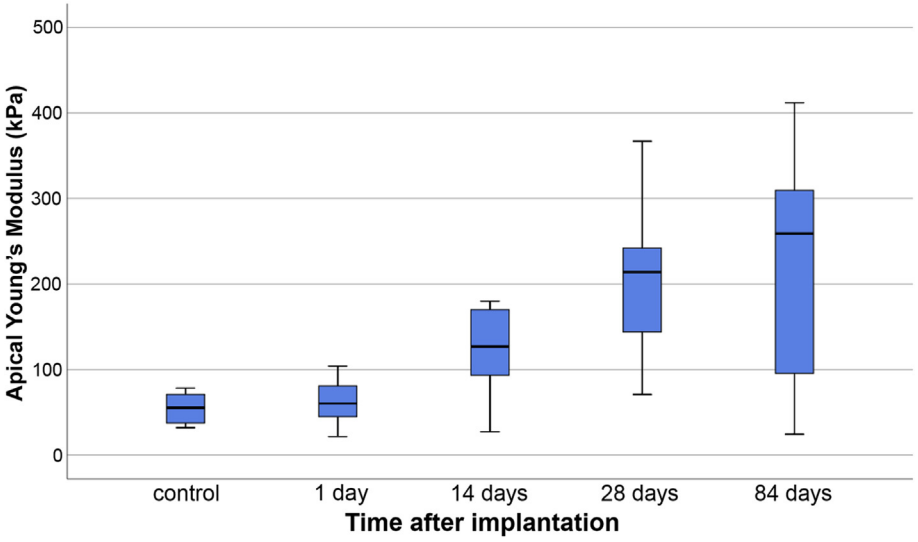

Fig. 7. Progressive stiffening of the apical basilar membrane tissue is seen from 1 day post-implantation until the last recorded time point of 84 days. Shown as boxplots and inter-quartiles.

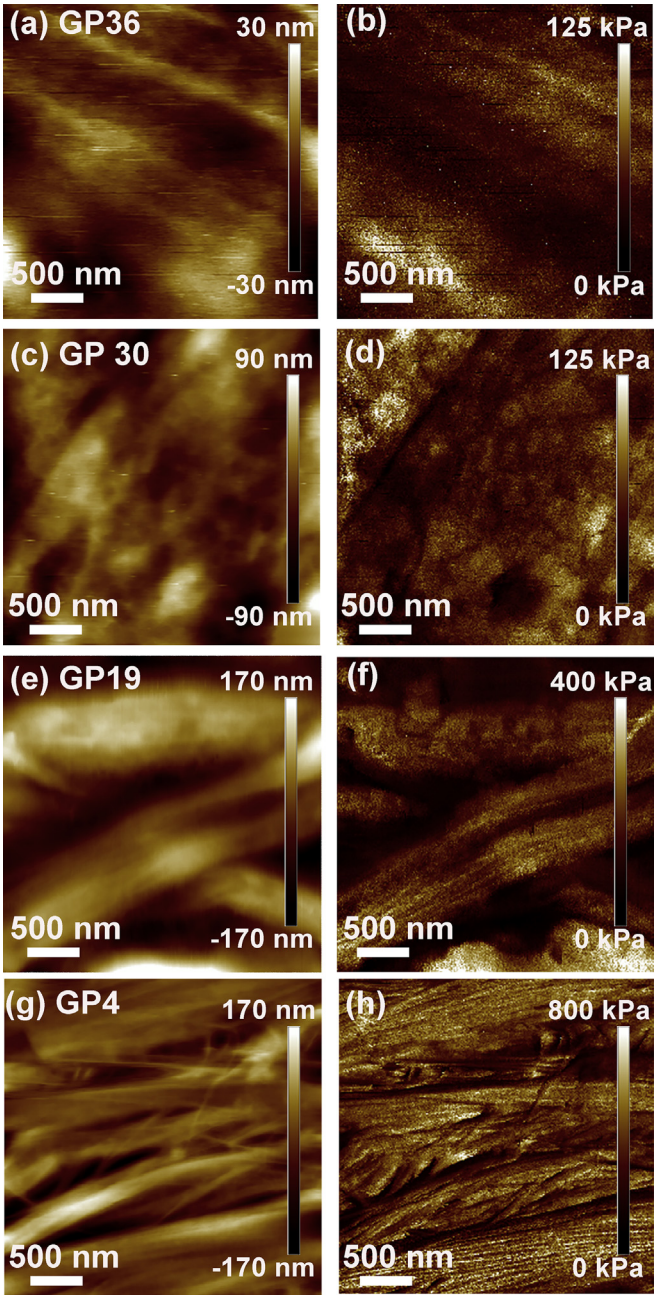

Fig. 8. QNM-AFM topography (a,c,e,g) and Young's modulus maps (b,d,f,h) of the apical basilar membrane of animals from 1 day (a,b), 14 days (c,d), 28 days (e,f), and 84 days (g,h) cohorts. Bundles of fibrillar structures were seen to appear over time and dominated the images by 84 days. The appearance of these bundles was similar to that seen of collagen fibrils in previous studies. *GP* is an animal identifier.

2013; Smeds et al., 2015), and endolymphatic hydrops has been proposed as a possible etiology, as it is transient in most animals after CI surgery and maximal in the basal cochlea in the vicinity of the implant, in the region where the 8–32 kHz acoustic responses were generated (Smeds et al., 2015). The partial recovery of hearing highlights the likely involvement of several mechanisms in determining hearing outcomes after CI surgery.

5. Conclusions

We observed a progressive stiffening of the BM occurring over 84 days after implantation. This progressive stiffening was observed in the apical regions of the cochlea. AFM topographic mapping was consistent with micro-calcification in the basal cochlea, and micro-scarring in BM derived from the apical cochlea. Collagen fibrils are extremely stiff, and their deposition on the BM is the likely molecular basis for the BM stiffening we observed. These findings provide evidence that cochlear implantation causes micro-scarring throughout the cochlea and introduces new observations that might help to understand how the ensuing low-frequency hearing loss occurs.

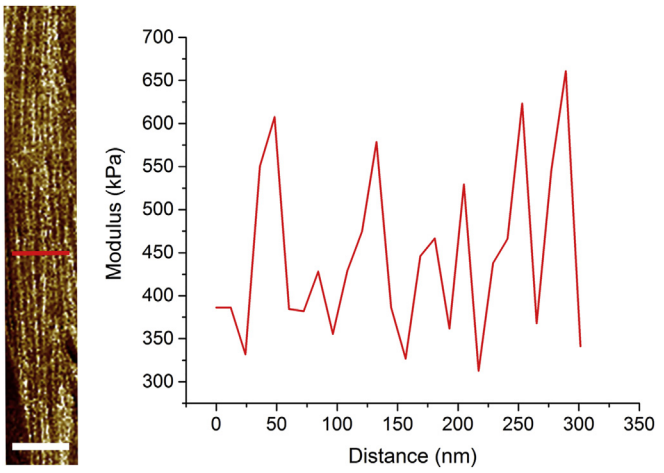

Fig. 9. Representative image used to quantify the Young's modulus of the fibrillar bundles seen in the apex of the BM after 84 days, scale bar = 300 nm. The cross-section bisects 5 fibrillar structures, which all had maximum stiffness between 550 and 700 kPa. The mean fibril stiffness of 629 ± 15 kPa was calculated from 50 fibrils; the error is quoted as the standard error of the mean. Images taken from the BM of GP 5.

Declaration of competing interest

The authors disclose no conflicts of interest.

Acknowledgements

SJO is funded by the National Health and Medical Research Council (Australia) GNT1125790 and GNT1078673. NPR would like to thank the Australian Research Council (IC140100023) and Swinburne University of Technology for funding. JC was a recipient of the Hugh Noel Puckle Scholarship from the University of Melbourne. This research was funded by the Garnett Passe and Rodney Williams Memorial Foundation and a generous bequest from the family of the late Gordon Darling, AC.

Appendix A. Supplementary data

Supplementary data to this article can be found online at https://doi.org/10.1016/j.heares.2019.107846.

References

Anderson, H.C., 2003. Matrix vesicles and calcification. Curr. Rheumatol. Rep. 5, 222–226.
Briggs, R.J.S., Tykocinski, M., Saunders, E., Hellier, W., Dahm, M., Pyman, B., Clarke, G.M., 2013. Surgical implications of perimodiolar cochlear implant electrode design: avoiding intracochlear damage and scala vestibuli insertion. Cochlear Implants Int. 2, 135–149.
Campbell, L., Kaicer, A., Sly, D., Iseli, C., Wei, B., Briggs, R., O'Leary, S., 2016. Intra-operative real-time cochlear response telemetry predicts hearing preservation in cochlear implantation. Otol. Neurotol. 7, 332–338.
Carlstrom, D., Engfeldt, B., Engstrom, A., Ringertz, N.R., 1953. Studies on the chemical composition of normal and abnormal blood vessel walls. I. Chemical nature of vascular calcified deposits. Lab. Investig. 2, 325–335.

Choi, C.-H., Oghalai, J.S., 2005. Predicting the effect of post-implant cochlear fibrosis on residual hearing. Hear. Res. 205, 193–200.
Choong, J.K.L., Lo, J., Chambers, S.A., Hampson, A.J., Eastwood, H.T., O'Leary, S.J., 2019. Intracochlear tPA infusion may reduce fibrosis caused by cochlear implantation surgery. Acta Otolaryngol. 139, 396–402.
Chung, P.C., Glynos, E., Green, P.F., 2014. The elastic mechanical response of supported thin polymer films. Langmuir 30, 15200–15205.
Contiguglia, S.R., Alfrey, A.C., Miller, N.L., Runnells, D.E., Le Geros, R.Z., 1973. Nature of soft tissue calcification in uremia. Kidney Int. 4, 229–235.
Ehrlich, H.P., Hunt, T.K., 2012. Collagen organization critical role in wound contraction. Adv. Wound Care 1, 3–9.
Emadi, G., Richter, C.P., 2008. Developmental changes of mechanics measured in the gerbil cochlea. J. Assoc. Res. Otolaryngol. 9, 22–32.
Emadi, G., Richter, C.P., Dallos, P., 2004. Stiffness of the gerbil basilar membrane: radial and longitudinal variations. J. Neurophysiol. 91, 474–488.
Eshraghi, A.A., Van De Water, T.R., 2006. Cochlear implantation trauma and noise-induced hearing loss: apoptosis and therapeutic strategies. Anat. Rec. Part A 288A, 473–481.
Fayad, J.N., Makarem, A.O., Linthicum, F.H., 2009. Histopathologic assessment of fibrosis and new bone formation in implanted human temporal bones using 3D reconstruction. Otolaryngol. Head Neck Surg. 141, 247–252.
Fleischer, M., Schmidt, R., Gummer, A.W., 2010. Compliance profiles derived from a three-dimensional finite-element model of the basilar membrane. J. Acoust. Soc. Am. 127, 2973–2991.
Frye, M.D., Zhang, C., Hu, B.H., 2018. Lower level noise exposure that produces only TTS modulates the immune homeostasis of cochlear macrophages. J. Neuroimmunol. 323, 152–166.
Gantz, B.J., Turner, C., Gfeller, K.E., Lowder, M.W., 2005. Preservation of hearing in cochlear implant surgery: advantages of combined electrical and acoustical speech processing. The Laryngoscope 115, 796–802.
Gavara, N., Chadwick, R.S., 2010. Noncontact microrheology at acoustic frequencies using frequency-modulated atomic force microscopy. Nat. Methods 7, 650–654.
Gilbert, J., Charnley, M., Cheng, C., Reynolds, N.P., Jones, O.G., 2017. Quantifying Young's moduli of protein fibrils and particles with bimodal force spectroscopy. Biointerphases 12, 041001.
Graham, H.K., Hodson, N.W., Hoyland, J.A., Millward-Sadler, S.J., Garrod, D., Scothern, A., Griffiths, C.E., Watson, R.E., Cox, T.R., Erier, J.T., Trafford, A.W., Sherratt, M.J., 2010. Tissue section AFM: in situ ultrastructural imaging of native biomolecules. Matrix Biol. 29, 254–260.
Gstoettner, W.K., Helbig, S., Maier, N., Keifer, J., Radeloff, A., Adunka, O.F., 2006. Ipsilateral electric acoustic stimulation of the auditory system: results of long-term hearing preservation. Audiol. Neuro. Otol. 11 (Suppl. 1), 49–56.
Gummer, A.W., Johnstone, B.M., Armstrong, N.J., 1981. Direct measurement of basilar membrane stiffness in the Guinea pig. J. Acoust. Soc. Am. 70, 1298–1309.
Haake, S.M., Dinh, C.T., Chen, S., Eshraghi, A.A., Van De Water, T.R., 2009. Dexamethasone protects auditory hair cells against TNFα-initiated apoptosis via activation of PI3K/Akt and NFκB signaling. Hear. Res. 255, 22–32.
Hassenkam, T., Fantner, G.E., Cutroni, J.A., Weaver, J.C., Morse, D.E., Hansma, P.K., 2004. High-resolution AFM imaging of intact and fractured trabecular bone. Bone 35, 4–10.
James, D.P., Eastwood, H., Richardson, R., O'Leary, S.J., 2008. Effects of round window dexamethasone on residual hearing in a Guinea pig model of cochlear implantation. Audiol. Neurotol. 13, 86–96.
Kel, G.E., Tan, J., Eastwood, H.T., Wongprasartsuk, S., O'Leary, S.J., 2013. Early cochlear response and ICAM-1 expression to cochlear implantation. Otol. Neurotol. 34, 1595–1602.
Kiefer, J., Böhnke, F., Adunka, O., Arnold, W., 2006. Representation of acoustic signals in the human cochlea in presence of a cochlear implant electrode. Hear. Res. 221, 36–43.
Kuznetsova, T.G., Starodubtseva, M.N., Yegorenkov, N.I., Chizhik, S.A., Zhdanov, R.I., 2007. Atomic force microscopy probing of cell elasticity. Micron 38, 824–833.
Lee, J., Ismail, H., Lee, J.H., Kel, G., O'Leary, J., Hampson, A., Eastwood, H., O'Leary, S.J., 2013. Effect of both local and systemically administered dexamethasone on long-term hearing and tissue response in a Guinea pig model of cochlear implantation. Audiol. Neurotol. 18, 392–405.
Lehnhardt, E., 1993. Intracochlear placement of cochlear implant electrodes in soft surgery technique. HNO 41, 356–359.
Li, P.M.M.C., Somdas, M.A., Eddington, D.K., Nadol Jr., J.B., 2007. Analysis of intracochlear new bone and fibrous tissue formation in human subjects with cochlear implants. Ann. Otol. Rhinol. Laryngol. 116, 731–738.
Linthicum, F.H., Doherty, J.K., Lopez, I.A., Ishiyama, A., 2017. Cochlear implant histopathology. World J. Otorhinolaryngol. Head Neck Surg. 3, 211–213.
Lo, J., Sale, P., Wijewickrema, S., Campbell, L., Eastwood, H., O'Leary, S.J., 2017. Defining the hook region anatomy of the Guinea pig cochlea for modelling of inner ear surgery. Otol. Neurotol. 38, e179–e189.
Lübbe, J., Temmen, M., Rahe, P., Kühnle, A., Reichling, M., 2013. Determining cantilever stiffness from thermal noise. Beilstein J. Nanotechnol. 4, 227–233.
Miller, C.E., 1985. Structural implications of basilar membrane compliance measurements. J. Acoust. Soc. Am. 77, 1465–1474.
Nadol Jr., J.B., Shiao, J.Y., Burgess, B.J., Ketten, D.R., Eddington, D.K., Gantz, B.J., Kos, I., Montandon, P., Coker, N.J., Roland Jr., J.T., Shallop, J.K., 2001. Histopathology of cochlear implants in humans. Ann. Otol. Rhinol. Laryngol. 110, 883–891.
Naidu, R.C., Mountain, D.C., 1998. Measurements of the stiffness map challenge a basic tenet of cochlear theories. Hear. Res. 124, 124–131.
O'Leary, S.J., Monksfield, P., Kel, G., Connolly, T., Souter, M.A., Chang, A., Marovic, P., O'Leary, J.S., Richardson, R., Eastwood, H., 2013. Relations between cochlear histopathology and hearing loss in experimental cochlear implantation. Hear. Res. 298, 27–35.
Olson, E.S., Mountain, D.C., 1991. In vivo measurement of basilar membrane stiffness. J. Acoust. Soc. Am. 89, 1262–1275.
Olson, E.S., Mountain, D.C., 1994. Mapping the cochlear partition's stiffness to its cellular architecture. J. Acoust. Soc. Am. 95, 395–400.
Oshima, H., Ikeda, R., Nomura, K., Yamazaki, M., Hidaka, H., Katori, Y., Oshima, T., Kawase, T., Kobayashi, T., 2014. Change in endocochlear potential during experimental insertion of a simulated cochlear implant electrode in the Guinea pig. Otol. Neurotol. 35, 234–240.
Radeloff, A., Unkelbach, M.H., Tillein, J., Braun, S., Helbig, S., Gstöttner, W., Adunka, O.F., 2007. Impact of intrascalar blood on hearing. The Laryngoscope 117, 58–62.
Ryu, K.A., Lyu, A.-R., Park, H., Choi, J.W., Hur, G.M., Park, Y.-H., 2015. Intracochlear bleeding enhances cochlear fibrosis and ossification: an animal study. PLoS One 10, e0136617.
Sharma, T., Radosevich, J.A., Pachori, G., Mandal, C.C., 2016. A molecular view of pathological microcalcification in breast cancer. J. Mammary Gland Biol. Neoplasia 21, 25–40.
Smeds, H., Eastwood, H.T., Hampson, A.J., Sale, P., Campbell, L.J., Arhatari, B.D., Mansour, S., O'Leary, S.J., 2015. Endolymphatic hydrops is prevalent in the first weeks following cochlear implantation. Hear. Res. 327, 48–57.
Stathopoulos, D., Chambers, S., Enke, Y.L., Timbol, G., Risi, F., Miller, C., Cowan, R., Newbold, C., 2014. Development of a safe dexamethasone-eluting electrode array for cochlear implantation. Cochlear Implants Int. 15, 254–263.
Teudt, I.U., Richter, C.P., 2014. Basilar membrane and tectorial membrane stiffness in the CBA/CaJ mouse. J. Assoc. Res. Otolaryngol. 15, 675–694.
Thurner, P.J., Oroudjev, E., Jungmann, R., Kreutz, C., Kindt, J.H., Schitter, G., Okouneva, T.O., Lauer, M.E., Fantner, G.E., Hansma, H.G., Hansma, P.K., 2007. Imaging of bone ultrastructure using atomic force microscopy. In: Méndez-Vilas, A., Diaz, J. (Eds.), Modern Research and Educational Topics in Microscopy. FORMATEX, pp. 37–48.
Von Békésy, G., 1960. Experiments in Hearing. McGraw-Hill Book Company, New York.
Wenger, M.P.E., Bozec, L., Horton, M.A., Mesquida, P., 2007. Mechanical properties of collagen fibrils. Biophys. J. 93, 1255–1263.
Young, T.J., Monclus, M.A., Burnett, T.L., Broughton, W.R., Ogin, S.L., Smith, P.A., 2011. The use of the PeakForce™ quantitative nanomechanical mapping AFM-based method for high-resolution Young's modulus measurement of polymers. Meas. Sci. Technol. 22, 125703.